

Dartmouth College

Dartmouth Digital Commons

Dartmouth Scholarship

Faculty Work

9-2015

Bypassing Iron Storage in Endodermal Vacuoles Rescues the Iron Mobilization Defect in the Natural Resistance Associated-Macrophage Protein3natural Resistance Associated-Macrophage Protein4 Double Mutant


Viviane Mary
Université Paris-Saclay

Magali Schnell Ramos
Université Paris-Saclay

Cynthia Gillet
Université Paris-Saclay

Amanda L. Socha
Dartmouth College

Jerome Giraudat
Université Paris-Saclay
Follow this and additional works at: <https://digitalcommons.dartmouth.edu/facoa>

 Part of the [Plant Sciences Commons](#)
See next page for additional authors

Dartmouth Digital Commons Citation

Mary, Viviane; Ramos, Magali Schnell; Gillet, Cynthia; Socha, Amanda L.; Giraudat, Jerome; Agorio, Astrid; Merlot, Sylvain; Clairet, Colin; Kim, Sun A.; Punshon, Tracy; Guerinot, Mary Lou; and Thomine, Sebastien, "Bypassing Iron Storage in Endodermal Vacuoles Rescues the Iron Mobilization Defect in the Natural Resistance Associated-Macrophage Protein3natural Resistance Associated-Macrophage Protein4 Double Mutant" (2015). *Dartmouth Scholarship*. 3671.
<https://digitalcommons.dartmouth.edu/facoa/3671>

This Article is brought to you for free and open access by the Faculty Work at Dartmouth Digital Commons. It has been accepted for inclusion in Dartmouth Scholarship by an authorized administrator of Dartmouth Digital Commons. For more information, please contact dartmouthdigitalcommons@groups.dartmouth.edu.

Authors

Viviane Mary, Magali Schnell Ramos, Cynthia Gillet, Amanda L. Socha, Jerome Giraudat, Astrid Agorio, Sylvain Merlot, Colin Clairet, Sun A. Kim, Tracy Punshon, Mary Lou Guerinot, and Sebastien Thomine

Bypassing Iron Storage in Endodermal Vacuoles Rescues the Iron Mobilization Defect in the *natural resistance associated-macrophage protein3* *natural resistance associated-macrophage protein4* Double Mutant¹[OPEN]

Viviane Mary, Magali Schnell Ramos, Cynthia Gillet, Amanda L. Socha, Jérôme Giraudat, Astrid Agorio, Sylvain Merlot, Colin Clairet, Sun A. Kim, Tracy Punshon, Mary Lou Guerinot, and Sébastien Thomine*

Institute for Integrative Biology of the Cell, Saclay Plant Sciences, Université Paris-Saclay, Commissariat à l'Energie Atomique, Centre National de la Recherche Scientifique, Université Paris-Sud, F-91198 Gif-sur-Yvette, France (V.M., M.S.R., C.G., J.G., A.A., S.M., C.C., S.T.); and Department of Biological Sciences, Dartmouth College, Hanover, New Hampshire 03755 (A.L.S., S.A.K., T.P., M.L.G.)

ORCID ID: 0000-0001-9603-7710 (A.A.).

To improve seed iron (Fe) content and bioavailability, it is crucial to decipher the mechanisms that control Fe storage during seed development. In *Arabidopsis thaliana* seeds, most Fe is concentrated in insoluble precipitates, with phytate in the vacuoles of cells surrounding the vasculature of the embryo. NATURAL RESISTANCE ASSOCIATED-MACROPHAGE PROTEIN3 (AtNRAMP3) and AtNRAMP4 function redundantly in Fe retrieval from vacuoles during germination. When germinated under Fe-deficient conditions, development of the *nramp3nramp4* double mutant is arrested as a consequence of impaired Fe mobilization. To identify novel genes involved in seed Fe homeostasis, we screened an ethyl methanesulfonate-mutagenized population of *nramp3nramp4* seedlings for mutations suppressing their phenotypes on low Fe. Here, we report that, among the suppressors, two independent mutations in the VACUOLAR IRON TRANSPORTER1 (AtVIT1) gene caused the suppressor phenotype. The AtVIT1 transporter is involved in Fe influx into vacuoles of endodermal and bundle sheath cells. This result establishes a functional link between Fe loading in vacuoles by AtVIT1 and its remobilization by AtNRAMP3 and AtNRAMP4. Moreover, analysis of subcellular Fe localization indicates that simultaneous disruption of AtVIT1, AtNRAMP3, and AtNRAMP4 limits Fe accumulation in vacuolar globoids.

Iron (Fe) is an essential micronutrient. In cells, this metal may change between two oxidation states: ferrous (Fe²⁺) and ferric (Fe³⁺). This property makes Fe an important metal cofactor for electron transfer in many biochemical reactions. However, for the same reason,

free Fe generates harmful reactive oxygen species via the Fenton reaction (Haber and Weiss, 1932; Halliwell, 1978). Cells thus need to tightly control Fe homeostasis through chelation and compartmentalization. For example, in yeast (*Saccharomyces cerevisiae*), the membrane transporter yeast Calcium-sensitive Cross-Complementer1 (ScCCC1) is required to move excess Fe into the vacuole (Li et al., 2001). The $\Delta ccc1$ mutant is sensitive to extracellular Fe. In mammalian cells, excess cytosolic Fe is complexed by ferritins; the assembly of 24 ferritin monomers forms a hollow complex able to safely store up to 4,500 Fe(III) atoms (Finazzi and Arosio, 2014).

Fe deficiency is an important public health issue: 2 billion people, corresponding to over 25% of the world population, are anemic (World Health Organization, 2015). To fight Fe deficiency, it has been proposed to develop crops with more available Fe according to a strategy called biofortification (Bouis, 2003). In most crops, seeds are used as food or feed. Fe stores in seeds are also important for the germination of seedlings. In seeds, Fe may be associated with ferritin in plastids, with phytate in vacuoles, or with nicotianamine. Although Fe complexed with ferritin or nicotianamine is considered highly bioavailable, Fe phytate is insoluble and poorly bioavailable (Clemens, 2014).

¹ This work was supported by the Centre National de la Recherche Scientifique (grant nos. ANR-07-BLAN-0110 and ANR-2011-BSV6-00401 to S.T.), by the Université Paris-Sud (doctoral grant to V.M.), by the National Institute of Environmental Health Services (grant no. P42 ES007373 to M.L.G. and T.P.), and by the National Science Foundation (grant nos. IOS-0919941 and DBI-0701119 to M.L.G.). GeoSoilEnviro-CARS is supported by the National Science Foundation (EAR-1128799) and the Department of Energy-Geosciences (DE-FG02-94ER14466).

* Address correspondence to sebastien.thomine@i2bc.paris-saclay.fr.

The author responsible for distribution of materials integral to the findings presented in this article in accordance with the policy described in the Instructions for Authors (www.plantphysiol.org) is: Sébastien Thomine (sebastien.thomine@i2bc.paris-saclay.fr).

V.M., M.S.R., C.G., A.L.S., J.G., A.A., and C.C. performed the experiments and analyzed the data; S.M., T.P., M.L.G., and S.T. designed and supervised the experiments and analyzed the data; S.A.K. and M.L.G. provided unpublished material and critical reading of the article; V.M. and S.T. wrote the article.

[OPEN] Articles can be viewed without a subscription.

www.plantphysiol.org/cgi/doi/10.1104/pp.15.00380

In *Arabidopsis* (*Arabidopsis thaliana*) seeds, no more than 5% of the total seed Fe is associated with ferritin (Ravet et al., 2009). About 50% of seed Fe is concentrated in the vacuoles of endodermal and bundle sheath cells surrounding the vasculature in the radicle and cotyledons of the embryo, respectively (Lanquar et al., 2005; Kim et al., 2006; Roschztardt et al., 2009; Schnell Ramos et al., 2013). As endodermal and bundle sheath cells belong to the same lineage, they will be collectively referred to as endodermal cells in this report. VACUOLAR IRON TRANSPORTER1 (*AtVIT1*) is responsible for the loading of Fe in endodermal vacuoles during seed development (Kim et al., 2006). *VIT1* is homologous to CCC1, which mediates Fe sequestration in the vacuole in yeast (Li et al., 2001). In addition to *VIT1*, which is mostly expressed during seed development, the *Arabidopsis* genome encodes five *VIT1*-like proteins (*VTLs*). *VTL* gene expression is down-regulated under Fe deficiency (Gollhofer et al., 2011). At least one of the *VTLs* also functions in Fe sequestration in the vacuole (Gollhofer et al., 2014). *VIT1* homologs have been identified in most plant species for which genome sequencing data are available. In rice (*Oryza sativa*), *OsVIT1* and *OsVIT2* sequester Fe and zinc in the vacuole of the flag leaf (Zhang et al., 2012). Loss of *AtVIT1* function perturbs the cell type-specific localization of Fe in mature embryos. Accordingly, in the *vit1-1* knockout mutant, Fe is no longer concentrated in cells surrounding the vasculature of the hypocotyl, radicle, and cotyledons but instead is accumulated in cortical cells in the hypocotyl and radicle and in the subepidermal cells of the abaxial side of cotyledons (Kim et al., 2006). Loss of *AtVIT1* function also has an impact on germination on alkaline (pH 7.9) soil: *vit1-1* mutant seedlings grow poorly compared with the wild type (Kim et al., 2006).

NATURAL RESISTANCE ASSOCIATED-MACROPHAGE PROTEIN3 (*AtNRAMP3*) and *AtNRAMP4* function redundantly in the mobilization of seed Fe from vacuoles during germination (Lanquar et al., 2005). They belong to a ubiquitous family of divalent cation transporters represented in all kingdoms of life. *NRAMP* proteins have well-documented roles in manganese (Mn) uptake in bacteria, yeast, and *Arabidopsis* (Nevo and Nelson, 2006; Cailliatte et al., 2010). In mammals, *NRAMP2/ Divalent Cation Transporter1/ Divalent Metal Transporter1* is the major uptake system involved in dietary Fe absorption (Andrews, 2004). Recently, some members of this family have been shown to transport other substrates (Xia et al., 2010; Ishikawa et al., 2012; Shin et al., 2014). The *Arabidopsis* genome encodes six *NRAMP* homologs. *AtNRAMP3* and *AtNRAMP4* are targeted to the vacuole and play a role in essential metal remobilization from this organelle, not only during seed germination but also in adult plants (Lanquar et al., 2005, 2010). Even though Fe content and localization are unaffected in mature seeds of the *nramp3nramp4* (*nr3nr4*) double knockout mutant (Schnell Ramos et al., 2013), seedlings of this mutant display strong defects when grown on an Fe-deficient medium: they are chlorotic

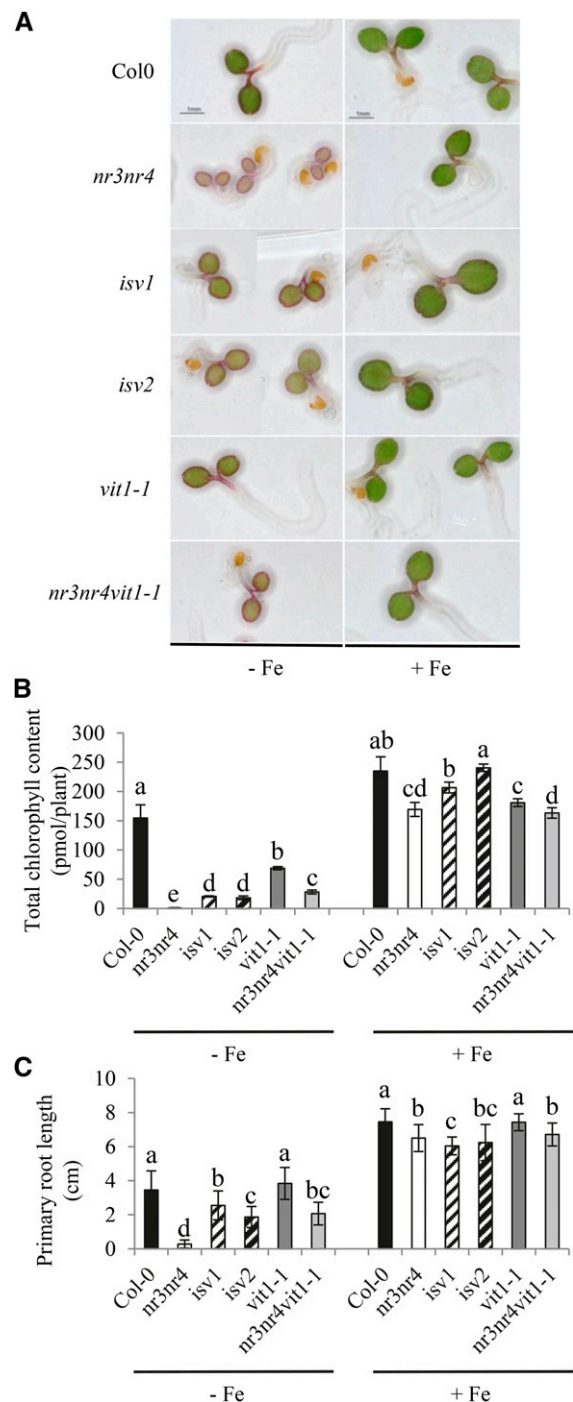


Figure 1. *isv1* (*nr3nr4vit1-2*), *isv2* (*nr3nr4vit1-3*), and *nr3nr4vit1-1* suppress chlorosis and developmental arrest phenotypes of *nr3nr4* on low-Fe medium after germination. **A**, Seedlings of the wild type (Columbia-0 [Col-0]), *nr3nr4*, *vit1-1*, *nr3nr4vit1-1*, *isv1*, and *isv2* grown for 5 d on ABIS medium without Fe (–Fe + 50 μM ferrozine) or with Fe (+50 μM Fe). Bars = 1 mm. **B**, Total chlorophyll content in seedlings grown as in **A** (mean \pm SE; $n = 3$ –6). **C**, Primary root length (mean \pm SE; $n = 16$ –40) of 12-d-old seedlings grown in ABIS medium without Fe (–Fe) or with Fe (+50 μM Fe). Different letters denote statistically significant differences between samples based on a Kruskal-Wallis test ($P < 0.001$) followed by Tukey's post hoc analysis with $P < 0.05$.

and their development is arrested (Lanquar et al., 2005).

When associated with phytate in vacuolar globoids, Fe is insoluble and notoriously poorly available for animal nutrition (Clemens, 2014). To identify mutations that limit Fe storage in this compartment, we generated an ethyl methanesulfonate (EMS)-mutagenized population of the *nr3nr4* mutant and looked for mutations that restore growth on Fe-deficient medium. We called these mutants *isv* (for bypass iron storage in vacuoles).

Here, we report the characterization of two *isv* mutants displaying Fe distribution patterns similar to the *vit1-1* mutant. These mutants carry mutations in the *AtVIT1* gene. By genetic analysis, we demonstrate that the mutations in *AtVIT1* are loss-of-function alleles that are responsible for the suppression phenotype. The *vit1-2* allele in *isv1* carries an amino acid change in the *AtVIT1* protein leading to a nonfunctional protein, and the *vit1-3* allele in *isv2* modifies the first intron-splicing consensus sequence leading to nonfunctional RNAs or proteins. Whereas NRAMP3 and NRAMP4 are necessary for retrieving Fe from vacuoles in the wild-type background, they are not necessary for using Fe in a *VIT1* loss-of-function background. Actually, combining *nramp3*, *nramp4*, and *vit1* mutations modifies Fe localization at the tissue and subcellular levels. These changes likely account for the ability of *vit1* mutations to rescue Fe mobilization and growth in the *nr3nr4* background.

RESULTS

Identification of Mutants Displaying Restored Growth on Low Fe in a Mutagenized Population of *nr3nr4* Seedlings

Following screening of 288,000 M2 seeds representing the progeny of 18,000 M1 plants, we selected 127 candidates, of which 32 suppressors could be confirmed at the M3 generation. To classify the candidates, the Fe distribution pattern of their embryos was determined using Perls enhanced by 3,3'-diaminobenzidine (Perls/DAB) staining (Roschztardt et al., 2009). On this basis, three classes could be established: most candidates displayed an Fe distribution pattern similar to the wild type; in some candidates, no staining could be observed; and three candidates displayed a non-wild-type Fe distribution pattern.

Identification of Two Novel *vit1* Mutant Alleles on the Basis of Their Fe Distribution Pattern

Among the candidates, we focused on *isv1* and *isv2*, which both display perturbed Fe distribution in their embryos. In both *isv1* and *isv2*, chlorosis and developmental arrest phenotypes of the *nr3nr4* double mutant on low-Fe medium were partially suppressed (Fig. 1A). When germinated on Fe-sufficient medium, wild-type, *nr3nr4*, *isv1*, and *isv2* seedlings contained equal amounts of chlorophyll. In contrast, under Fe-deficient

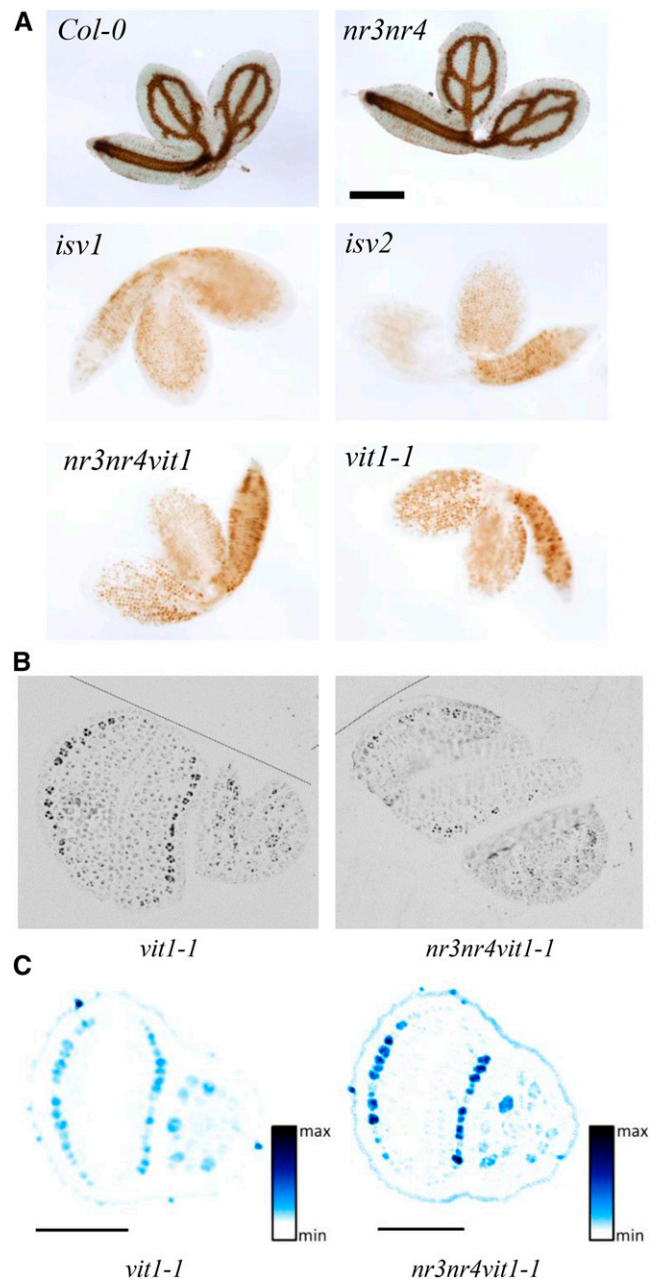


Figure 2. *isv1*, *isv2*, *vit1-1*, and *nr3nr4vit1-1* display similar Fe distribution patterns in embryos. A, Perls/DAB staining of whole embryos from *Col-0*, *nr3nr4*, *vit1-1*, *nr3nr4vit1-1*, *isv1*, and *isv2* mature seeds. Bar = 200 μ m. B, Perls/DAB staining on 3- μ m-thick transverse sections through embryos embedded in Epon resin. C, X-ray fluorescence microtomography of Fe K α fluorescence collected from intact mature *vit1-1* and *nr3nr4vit1-1* seeds. Bars = 100 μ m.

conditions, chlorophyll could not be detected in *nr3nr4*, whereas *isv1* and *isv2* seedlings contained 20.6 and 18.2 pmol of chlorophyll per plant, respectively, which corresponds to approximately 13% and 11% of the content measured in wild-type seedlings (*Col-0*) grown under the same conditions (Fig. 1B). To quantify the impact of *isv1* and *isv2* mutations on seedling development after

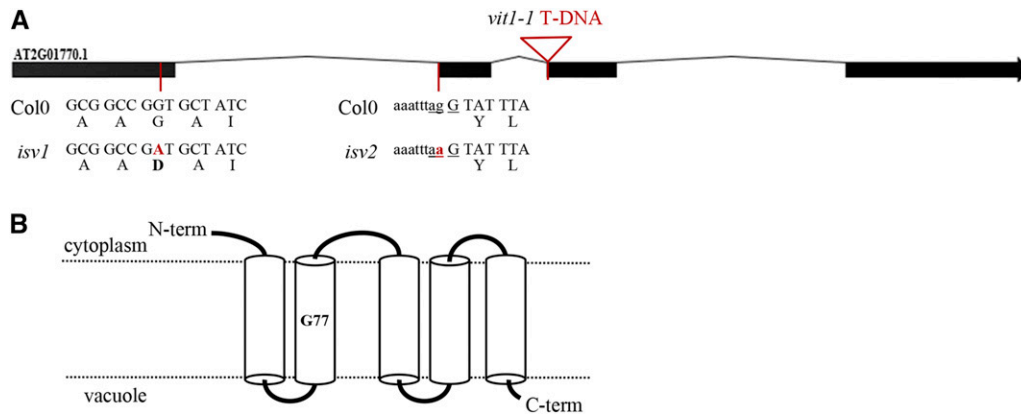


Figure 3. *isv1* and *isv2* carry mutations in the *VIT1* gene. A, Positions of *isv1* and *isv2* mutations and transfer DNA (T-DNA) insertion of the *vit1-1* mutant on the *VIT1* genomic DNA sequence (black bars stand for exons, black lines represent introns, and mutations are indicated in red). B, Predicted topology of the *VIT1* transporter. Gly-77 was localized in the middle of the second transmembrane domain.

germination, we measured the primary root length of 12-d-old seedlings. As expected, root length was similar for all the genotypes under Fe sufficiency. On $-Fe$ medium, *isv1* and *isv2* overcame the complete developmental arrest observed in *nr3nr4*, allowing root elongation to 74% and 54% of the wild-type level, respectively (Fig. 1C).

To determine whether *isv1* and *isv2* mutations are dominant or recessive, we backcrossed *isv1* and *isv2* with *nr3nr4*. On $-Fe$ medium, out of 90 seedlings of the F2 generation from the *isv1* \times *nr3nr4* cross, 26.6% showed a suppressor phenotype, and out of 94 seedlings of the F2 generation from the *isv2* \times *nr3nr4* cross, 20.2% showed a suppressor phenotype. The segregations observed are compatible with a recessive single locus based on χ^2 values of 0.71 for *isv1* and 0.28 *isv2*.

Figure 2A shows that *isv1* and *isv2* mutant embryos display Fe distribution patterns very similar to the pattern reported for the *vit1-1* mutant (Roschttardt et al., 2009). We thus tested whether *isv1* and *isv2* carry a mutation in the *AtVIT1* gene. We amplified and sequenced the *VIT1* gene in *isv1*, *isv2*, and the wild type. Sequence analysis revealed that *isv1* and *isv2* carry two different point mutations consistent with EMS mutagenesis in the *VIT1* genomic sequence (Fig. 3A). In *isv1*, a change from G to A at nucleotide 243 led to an amino acid change in the second predicted transmembrane domain: Gly-77 was replaced by an Asp (Fig. 3B). In *isv2*, a G-to-A conversion at nucleotide 699 affected the predicted acceptor site for the splicing of the first intron.

The Triple Knockout Mutant *nr3nr4vit1-1* Recapitulated the Phenotype of *isv1* and *isv2* on Low-Fe Medium

To test whether the loss of *VIT1* function could suppress the *nr3nr4* phenotype, we constructed the *nr3nr4vit1-1* triple mutant by combining knockout insertion alleles of the three genes. On Fe-deficient medium,

the triple knockout mutant displayed a phenotype intermediate between the wild-type Col-0 and *nr3nr4* (Fig. 1), similar to *isv1* and *isv2*. In agreement with a previous report showing a growth defect on alkaline soil (Kim et al., 2006), *vit1-1* single mutant growth and greening were also impaired on Fe-deficient medium. Its phenotype was intermediate between Col-0 and the triple mutant *nr3nr4vit1-1*. On Fe-sufficient medium, *vit1-1* was indistinguishable from wild-type Col-0 (Fig. 1). The Fe distribution pattern revealed by Perls/DAB staining of *nr3nr4vit1-1* whole embryos was similar to the Fe pattern in the *vit1-1* single mutant, as observed in *isv1* and *isv2* (Fig. 2A). Perls/DAB staining and micro Particle Induced X-ray Emission (μ PIXE) spectroscopy analyses of embryo sections as well as synchrotron x-ray

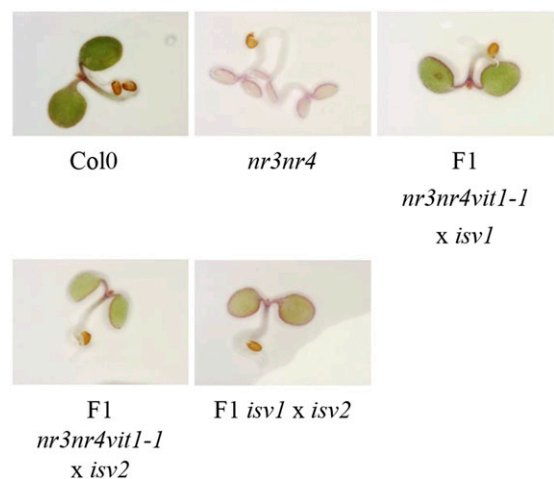


Figure 4. The suppressor phenotype of *isv1* (*nr3nr4vit1-2*) and *isv2* (*nr3nr4vit1-3*) candidates is caused by the mutations in *VIT1*. Photographs show the wild type, *nr3nr4*, and F1 seedlings from crosses between *nr3nr4vit1-1* and *isv1*, *nr3nr4vit1-1* and *isv2*, or *isv1* and *isv2* grown for 4 d on ABIS medium without Fe ($-Fe + 50 \mu M$ ferrozine).

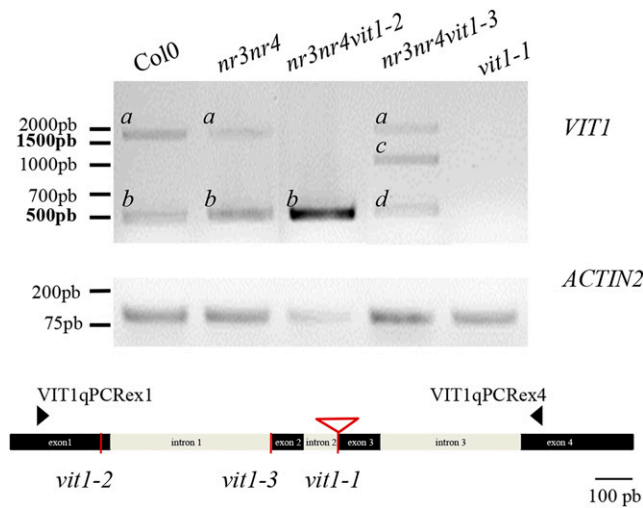


Figure 5. Effects of *vit1-2* and *vit1-3* mutations on *VIT1* mRNA structure. RT-PCR was performed on complementary DNA (cDNA) from siliques of *nr3nr4*, *nr3nr4vit1-1*, *nr3nr4vit1-2*, and *nr3nr4vit1-3*. Four different types of amplicons were detected and sequenced: a, residual genomic DNA or unspliced RNA; b, mature mRNA; c, mRNA with an unspliced first intron; and d, misspliced mRNA missing eight nucleotides at the beginning of the second exon.

fluorescence (SXRF) tomography of intact seeds confirmed that, in *nr3nr4vit1-1* embryos, Fe is concentrated in cotyledon abaxial subepidermal cells and radicle cortical cells, as in *vit1-1* (Fig. 2, B and C; Supplemental Fig. S1). These results establish that loss of VIT1 function suppresses the defects observed in the *nr3nr4* mutant germinated on low-Fe medium and that *nr3nr4vit1-1* has the same Fe distribution pattern in embryo tissues as *vit1-1*.

The Mutations in the *AtVIT1* Gene Sequence Are Responsible for the Suppressor Phenotype in *isv1* and *isv2* Mutants

To confirm that the EMS mutations found in the *AtVIT1* gene in *isv1* and *isv2* are responsible for the suppressor phenotype on low-Fe medium, we performed an allelic complementation test by crossing the triple knockout mutant *nr3nr4vit1-1* with *isv1* and with *isv2*. Allelic complementation tests establish whether two recessive mutations are in the same or in different genes. If the recessive mutations are in the same gene, the F1 generation is expected to display the suppressor phenotype. We sowed F1 generation seeds from *nr3nr4vit1-1* × *isv1*, *nr3nr4vit1-1* × *isv2*, and *isv1* × *isv2* crosses on $-Fe$ medium (Fig. 4) and observed that all seedlings displayed an intermediate phenotype reminiscent of the *nr3nr4vit1* triple knockout or the *isv1* and *isv2* mutants (Fig. 4). Taken together, these results establish a causal link between the *isv1* and *isv2* mutations found in the *VIT1* gene and their suppressor phenotype in *nr3nr4vit1-2* and *nr3nr4vit1-3*, respectively.

The *vit1-3* Mutation Prevents the Production of Functional *AtVIT1* mRNA in *isv2*

As *isv2* (*nr3nr4vit1-3*) mutants carry a mutation in the acceptor site involved in the splicing of the first intron of *VIT1*, we investigated the effect of the *vit1-3* mutation on *VIT1* mRNA using reverse transcription (RT)-PCR. Experiments were carried out using primers that amplify a fragment of *VIT1* spanning all three introns, with *ACTIN2* as a reference gene. The results presented in Figure 5 show an amplicon at the expected size (461 bp) for the spliced transcript in Col-0 and the *nr3nr4* double mutant (band b) and no amplification at this size in *vit1-1*. The high molecular mass band observed in Col-0, *nr3nr4*, and *nr3nr4vit1-3* (band a) corresponds to the size of the genomic DNA (1,359 bp) or to an unspliced version of the mRNA. An amplicon at the expected size (461 bp) for the spliced transcript (band b) was also observed in *isv1* (*nr3nr4vit1-2*). In *nr3nr4vit1-3*, two amplicons were present in addition to band a, one matching the size of a modified form of the mRNA where the first intron is not spliced (band c; 893 bp) and one at the expected size for the properly spliced RNA (band d). Sequencing of these amplicons confirmed the identity of the high molecular mass band (band c) and revealed that, in the band at the correct size (band d), eight nucleotides are missing, introducing a frame shift in the cDNA (Supplemental Fig. S2). In contrast, the sequence of the amplicon at the same size (band b) in Col-0, *nr3nr4*, and *nr3nr4vit1-2* corresponds to the predicted cDNA. Both mRNAs detected in *nr3nr4vit1-3* contain premature stop codons and are predicted to give rise to proteins truncated after Tyr-90 and Ser-108. The *vit1-3* mutation led to the production of two non-functional mRNAs of *VIT1*, while the *vit1-2* mutation did not impair *VIT1* mRNA production.

The G77D Mutation Impairs the Ability of *AtVIT1* to Transport Fe in Yeast

To examine the Fe transport activity of *AtVIT1*^{G77D} (*vit1-2*), we compared the ability of *AtVIT1* and *AtVIT1*^{G77D} to complement the $\Delta ccc1$ yeast mutant on high-Fe medium. *AtVIT1* is a functional homolog of yeast ScCCC1 (Kim et al., 2006). The $\Delta ccc1$ mutant is sensitive to high extracellular Fe concentrations and fails to grow on medium containing elevated levels of Fe (Li et al., 2001). In agreement with a previous report (Kim et al., 2006), $\Delta ccc1$ growth on 5 or 10 mM FeSO₄ could be restored by the expression of *AtVIT1* or GFP-*AtVIT1* (Fig. 6A). In contrast, the $\Delta ccc1$ yeast strain transformed with *AtVIT1*^{G77D} or GFP-*AtVIT1*^{G77D} was not able to grow on medium supplemented with high concentrations of FeSO₄ (Fig. 6A). Accordingly, the expression of *AtVIT1*, but not of *AtVIT1*^{G77D}, restored Fe accumulation in $\Delta ccc1$ (Fig. 6B). Immunoblot analysis using anti-VIT1 antibody did not reveal any difference between native VIT1 and VIT1^{G77D} protein levels in $\Delta ccc1$ (Fig. 6C). Moreover, examination of GFP-VIT1 by confocal microscopy did not provide any indication

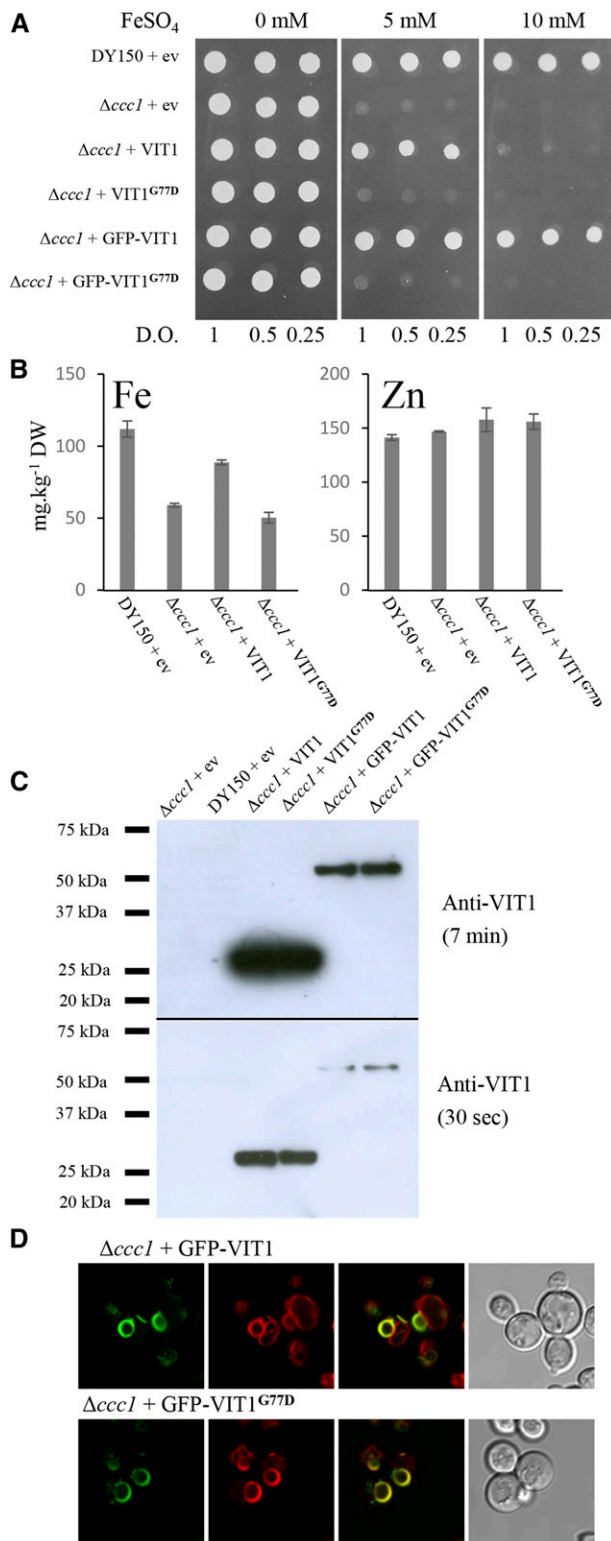


Figure 6. The VIT1 G77D transporter encoded by the *vit1-2* allele does not rescue the $\Delta ccc1$ yeast mutant. A, Yeast drop test. AtVIT1, AtVIT1^{G77D}, and their corresponding GFP fusion proteins were expressed in the $\Delta ccc1$ mutant. The complementation was scored by spotting serial dilutions of yeast transformants on selective medium (synthetic dextrose [SD]-Ura) supplemented or not with 5 or 10 mM

that the G77D mutation alters VIT1 localization (Fig. 6D). Together, these results suggest that Gly-77 is a critical residue for VIT1 Fe transport activity.

Subepidermal Fe Stores Are Efficiently Mobilized during Germination in the Absence of AtNRAMP3 and AtNRAMP4

To understand the mechanism by which mutations in AtVIT1 rescue the growth of *nr3nr4* mutant seedlings on low Fe, we examined the concentration and the fate of seed Fe stores in *nr3nr4vit1-1*. Measurements of Fe concentrations in seeds did not reveal any significant difference between Col-0, *nr3nr4*, *vit1-1*, and *nr3nr4vit1-1* (Supplemental Table S1). To monitor Fe mobilization, we performed Perls/DAB staining on seedlings grown on -Fe medium during the first 7 d after germination (Fig. 7). As reported previously (Roschztardt et al., 2009), in the wild type, the Perls/DAB staining around vascular tissues disappeared progressively after germination, indicating that Fe was mobilized (Fig. 7). In parallel, cotyledons became green after 4 d. In contrast, the strong staining surrounding the vasculature remained even after 7 d in *nr3nr4* double mutant seedlings, confirming that this mutant is unable to remobilize Fe, which was associated with extreme chlorosis and developmental arrest. In *vit1-1* and *nr3nr4vit1-1* mature embryos, Fe stores are located in the subepidermal cells on the abaxial side of the cotyledons and in the cortex of the radicle. During the first week of seedling development, the corresponding Perls/DAB staining disappeared with similar kinetics, indicating that Fe is efficiently mobilized in both single and triple mutants (Fig. 7). Accordingly, *vit1-1* and *nr3nr4vit1-1* mutants were able to grow on -Fe medium, and their cotyledons became green after 4 d. These data indicate that, in the *vit1-1* mutant background, Fe may be mobilized from subepidermal cells of cotyledons and in the cortex of the radicle even in the absence of NRAMP3 and NRAMP4. This result provides a mechanism for the suppressor effect of VIT1 loss-of-function mutations in *nr3nr4*.

Subcellular Localization of Fe in Cotyledon Subepidermal Cells

Our results indicated that Fe stored in cotyledon subepidermal cells is efficiently mobilized during germination in the absence of AtNRAMP3 and AtNRAMP4.

FeSO₄. The wild-type strain (DY150) and the $\Delta ccc1$ mutant transformed with an empty vector were used as controls. B, Fe and zinc (Zn) concentrations (mean \pm SE; *n* = 3) in the indicated yeast strains grown for 48 h in SD-Ura supplemented with 50 μ M FeSO₄. DW, Dry weight. C, Immunoblot analysis with antibody against VIT1 on protein extracts from strains used for the drop test. As the time for detection of the GFP fusion protein is longer than for the native version, two exposures are shown: 7 min (top) and 30 s (bottom). D, Localization of the GFP fluorescence signal in $\Delta ccc1$ yeast mutant cells transformed with the wild-type or G77D version of VIT1-GFP (green channel), FM4-64 (red channel), and overlay.

This raises the question of the compartment in which Fe is stored in the absence of VIT1. Is Fe localized in vacuolar globoids and mobilized by distinct vacuolar metal exporters, or is it stored in a different compartment? To address this question, we examined the subcellular localization of Fe and Mn in cotyledons from wild-type, *vit1-1*, and *nr3nr4vit1-1* triple mutant dry seeds using energy-dispersive x-ray (EDX) analysis coupled to transmission electron microscopy (TEM). No obvious difference in globoid density or size between genotypes was noted. Nevertheless, Fe and Mn signals in the globoids were normalized by the phosphorus $K\alpha$ signal, as phosphorus is the major component of globoids, to correct for variations in globoid size and number under the electron beam. As expected from previous work (Lanquar et al., 2005; Kim et al., 2006; Punshon et al., 2012; Schnell Ramos et al., 2013), Fe was highly concentrated in vacuolar globoids of endodermal cells in wild-type embryos. Mn could not be detected by EDX in this cell type and was concentrated in globoids from subepidermal cells (Figs. 8 and 9). Mn subcellular localization is consistent with a recent spectroscopic analysis demonstrating Mn association with phytate in seeds (Bruch et al., 2015). Fe was also detected in the cytosol of endodermal and subepidermal

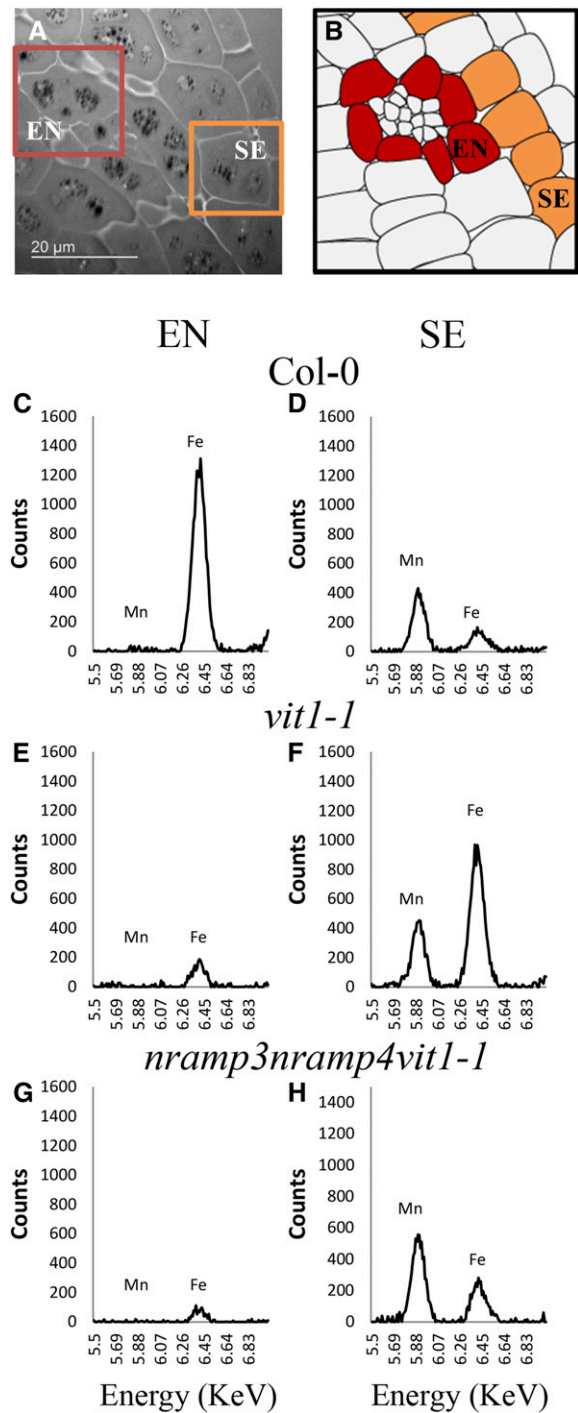


Figure 8. Less Fe is associated with vacuolar globoids of subepidermal cells in *nr3nr4vit1-1* than in the *vit1-1* mutant. Analysis of Fe and Mn contents was performed in vacuolar globoids in embryos from dry seeds using TEM-EDX. A, TEM micrograph of a 500-nm-thick transverse section through a cotyledon of a Col-0 embryo. B, Schematic representation of the section. EN, Endodermal/bundle sheath cell (red); SE, subepidermal cell (orange). C to H, Representative spectra of the energies of Mn and Fe emissions with beam focused on globoids from endodermal/bundle sheath cells (C, E, and G) or subepidermal cells (D, F, and H) in the wild type (C and D), *vit1-1* (E and F), or *nr3nr4vit1-1* (G and H).

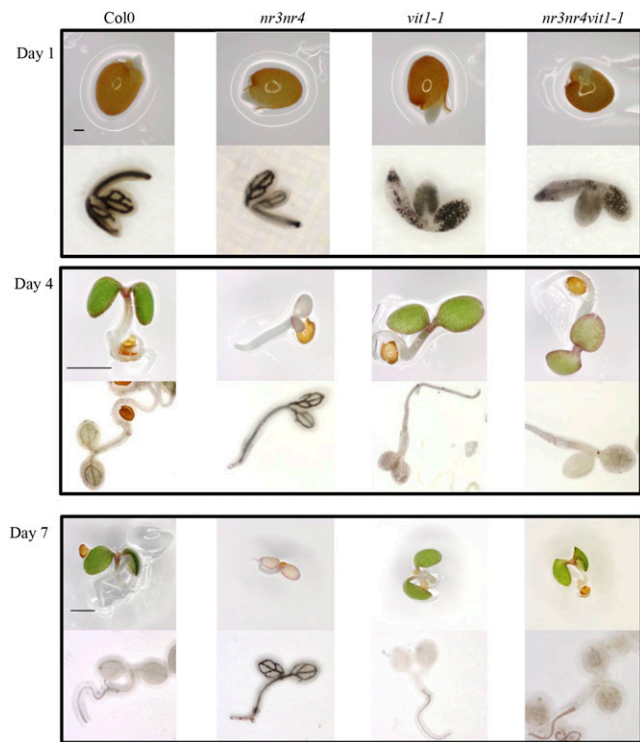


Figure 7. Fe stores are efficiently remobilized during *vit1-1* and *nr3nr4vit1-1* mutant seedling development. Seedling development and Fe localization were monitored in parallel during the first 7 d after sowing. For each section, images at the top show seedlings on low-Fe medium (ABIS -Fe + 50 μM ferrozine) and images at the bottom show Perl's/DAB staining of Col-0, *nr3nr4*, *vit1-1*, and *nr3nr4vit1-1* (from left to right) at 1, 4, or 7 d after transfer to the growth chamber. Bars = 100 μm (day 1), 1 mm (day 4), and 1 mm (day 7).

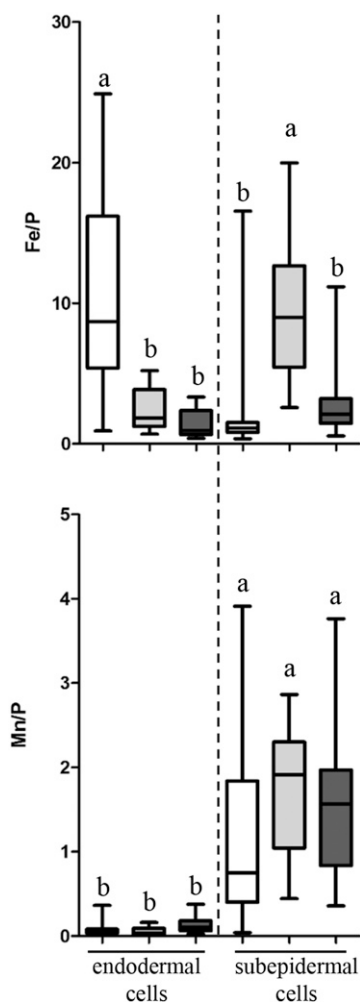


Figure 9. EDX analysis does not detect high Fe concentrations in *nr3nr4vit1-1* globoids of subepidermal cells. The value shown corresponds to 100 times the ratio Fe/P (or Mn/P). Ratios were calculated from integrated counts of Fe, Mn, and phosphorus (P) peaks in the spectra obtained by TEM-EDX in globoids of endodermal or subepidermal cells of cotyledons. Data are presented as medians, boxes show 25th and 75th percentiles, and whiskers show minimal and maximal values. White boxes, Col-0; light gray boxes, *vit1-1*; and dark gray boxes, *nr3nr4vit1-1*. Different letters denote statistically significant difference between samples ($n = 16\text{--}26$) based on a Kruskal-Wallis test ($P < 0.001$) followed by Tukey's post hoc analysis with $P < 0.05$.

cells as well as in subepidermal globoids, albeit at much lower levels than in endodermal cell globoids (Figs. 8 and 9). In *vit1-1* mutant embryos, Fe and Mn were both concentrated in subepidermal cell globoids. Nevertheless, Fe could still be detected at much lower levels in *vit1-1* endodermal cell globoids as well as in the cytosol of both subepidermal and endodermal cells. In contrast to the pattern revealed by Perls/DAB staining, μ PIXE, and SXRF in *vit1-1* and *nr3nr4vit1-1*, Fe was detected at low levels in globoids from subepidermal and endodermal cells in the triple mutant (Figs. 8 and 9). Together with the results of Perls/DAB analysis indicating that Fe is concentrated in subepidermal cells, these data suggest

that the subcellular localization of Fe is modified in *nr3nr4vit1-1* triple mutants. However, TEM-EDX did not detect any increase in Fe in the cytosol of subepidermal cells in *nr3nr4vit1-1* compared with *vit1-1* or the wild type (Supplemental Fig. S3). Mn distribution was not affected by the mutations. Mn was concentrated in subepidermal cell globoids in all the genotypes analyzed (Figs. 8 and 9). Interestingly, Mn was not present in all subepidermal cells: in about one-third of subepidermal cells, Mn was not detected in globoids. In contrast to Fe, Mn could not be detected in the cytosol, irrespective of the cell type analyzed (Supplemental Fig. S3).

DISCUSSION

In this work, we screened an EMS mutagenized population of *nr3nr4* double mutants looking for mutations that suppress its chlorotic phenotype under Fe deficiency. We characterized two mutants in which loss of VIT1 function is responsible for the suppressor phenotype (Fig. 4).

Novel Mutations Provide Insights into AtVIT1 Protein Structure-Function Relationships

Two distinct mutations were discovered in the *VIT1* gene. In *isv1*, the *vit1-2* mutation led to an amino acid change: Gly-77, a hydrophobic residue with no lateral chain, was replaced by Asp, a polar residue with a bulky lateral chain. The consensus topology for VIT1 provided in the ARAMEMNON membrane protein database predicts five α -helices forming transmembrane domains (Gollhofer et al., 2011; Fig. 3B). Gly-77 would be localized in the middle of the second transmembrane domain. Moreover, sequence alignment reveals that this transmembrane domain, and specifically Gly-77, is highly conserved in VIT1 homologs from a range of species (Supplemental Fig. S4). Previous studies have shown that the Δ *ccc1* growth defect may be rescued by transformation with *AtVIT1* and its homologs *AtVTL1* (Gollhofer et al., 2014), *LeVIT1* (Kim et al., 2006), *TgVIT1* (Momonoi et al., 2009), and *OsVIT1* or *OsVIT2* (Zhang et al., 2012). Expression in yeast indicates that the G77D mutation prevents Δ *ccc1* rescue by *AtVIT1* but does not alter the *AtVIT1* protein level or subcellular localization (Fig. 6). It is likely that Gly-77 might play a critical role in VIT1 transport function or indirectly in VIT1 interactions with membrane lipids, other transmembrane domains, or other proteins. Residues important for the function of VIT1 protein family proteins have already been identified (Hakoyama et al., 2012). Stationary Endosymbiont Nodule1 from *Lotus japonicus* (LjSEN1), a VIT1 homolog, is required for symbiotic nitrogen fixation by *Lotus japonicus*. Mutations A41V (*sen1-1*), R111K (*sen1-2*), and G191E (*sen1-5*) were shown to impair LjSEN1 function. However, whether these mutations affect LjSEN1 stability, localization, or transport function was not investigated, and none of these residues corresponds to Gly-77 in the LjSEN1 sequence (Supplemental Fig. S4).

In *iso2*, the *vit1-3* mutation led to a change in the 3' splicing consensus sequence of the first intron (Figs. 3 and 5). Two forms of RNA could be detected in *nr3nr4vit1-3*. In the first one, the first intron is unspliced, and in the other one, the intron is misspliced. For this second RNA form, a cryptic acceptor site located eight nucleotides downstream of the mutation in the second exon is used, which causes a frame shift (Fig. 5; Supplemental Fig. S2). Both RNA forms introduce premature stop codons and are expected to produce nonfunctional proteins. A mutation in a splicing acceptor site in Constitutive Photomorphogenesis1 (COP1; *cop1-11*) was previously shown to lead to a similar combination of nonfunctional mRNAs including unspliced and misspliced species (McNellis et al., 1994).

VIT1, AtNRAMP3, and AtNRAMP4 Define a Functional Module for Fe Storage in Endodermal Cells

To our knowledge, our study provides the first genetic evidence that AtVIT1, AtNRAMP3, and AtNRAMP4 function in the same pathway by demonstrating an epistatic relationship between *vit1* and *nr3nr4* mutations. In the wild-type embryo, about 50% of stored Fe is localized in endodermal cells, where AtVIT1, AtNRAMP3, and AtNRAMP4 are expressed (Lanquar et al., 2005; Kim et al., 2006). Our TEM-EDX data confirm that, in this cell type, the main site for Fe storage is the vacuole. Furthermore, this work indicates that the AtVIT1/AtNRAMP3/AtNRAMP4 functional module is essential for Fe storage in this specific cell type (Fig. 10). This module may be conserved in other species. In seeds of *Phaseolus* spp., Fe is also concentrated around vascular tissues, similar to the situation encountered in Arabidopsis seeds (Cvitanich et al., 2010). In cereals, such as rice or wheat (*Triticum aestivum*), a major part of seed Fe is stored in the aleurone layer (Johnson et al., 2011), and Fe was found to be associated with globoids in this cell layer in wheat (Lott and Spitzer, 1980). The molecular players

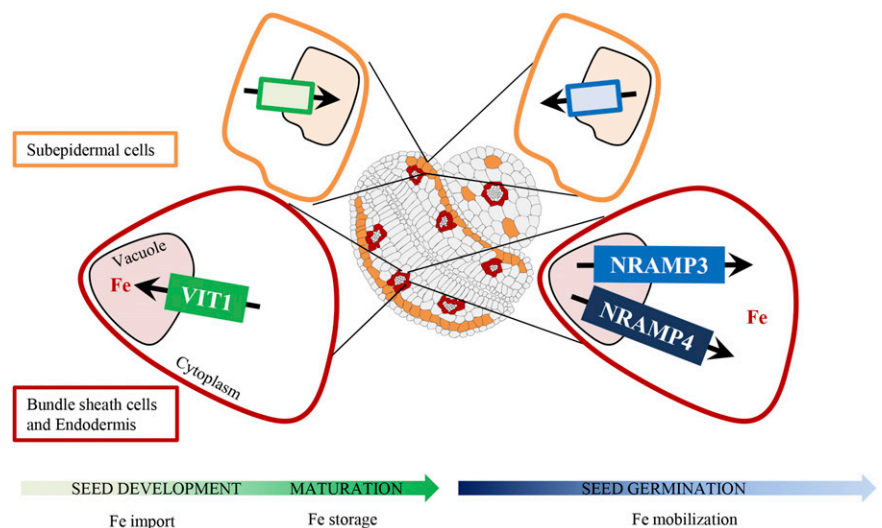
involved in loading and remobilization have not yet been identified in species other than Arabidopsis.

A Range of Phenotypes Associated with the Localization of Fe Stores in Embryos and Their Mobilization

The phenotypes observed on Fe-deficient medium may be ranked on the basis of their severity: wild type >> *vit1-1* > *nr3nr4vit1-1* = *nr3nr4vit1-2* = *nr3nr4vit1-3* >> *nr3nr4*. In our conditions, wild-type seedlings are not chlorotic under Fe-deficient conditions, at least not during the first week after germination (Fig. 1). This indicates that seed Fe stores are sufficient for the initial stages of development. At the other end, *nr3nr4* seedlings are highly chlorotic, and their development is fully arrested under Fe deficiency (Fig. 1). This confirms that retrieval of vacuolar Fe stores is essential for seedling development (Lanquar et al., 2005). As described previously (Kim et al., 2006), *vit1* seedlings were also chlorotic when germinated under Fe deficiency (Fig. 1). However, this phenotype was clearly milder than that of the *nr3nr4* double mutant: despite the chlorosis, *vit1-1* mutant roots reach the same size as the wild type after 2 weeks (Fig. 1C). Our results indicate that Fe is readily mobilized from cotyledon subepidermal cells and root cortical cells in *vit1-1* (Figs. 7 and 10). Therefore, the *vit1* phenotype did not result from a defect in Fe mobilization but rather from Fe being released in the wrong location.

Interestingly, *nr3nr4vit1-2* (*iso1*), *nr3nr4vit1-3* (*iso2*), and *nr3nr4vit1-1* triple knockout mutants displayed a phenotype intermediate between *vit1-1* and *nr3nr4*. Importantly, seedlings of these mutants contained detectable levels of chlorophyll and had elongated roots, which is not the case for the *nr3nr4* double mutant. Moreover, their Fe stores were mobilized from cotyledon subepidermal cells and root cortical cells as efficiently as in the *vit1-1* single mutant (Fig. 7). This indicates that

Figure 10. Working model for VIT1 and NRAMP3/NRAMP4 during seed development, maturation, and germination in Arabidopsis embryo (transverse section). Bundle sheath and endodermal cells are highlighted in red. Subepidermal cells are highlighted in orange. Vacuolar Fe transporters are represented as green or blue boxes.



these cell types mobilize Fe independently of AtNRAMP3 and AtNRAMP4 (Fig. 10).

The origin of the difference between the phenotypes of the *vit1-1* single mutant and the *nr3nr4vit1-1* triple mutant might reside in the remobilization of Fe from pools that are not visualized by Perls/DAB staining. Schnell Ramos et al. (2013) have reported that only 50% of Fe in the embryo is located in the highly concentrated areas of the endodermis in the wild type or in cotyledon subepidermal cells in *vit1-1*. However, Fe is present at lower concentrations in all embryo cell types. Whereas AtVIT1 expression is restricted to the vasculature (Kim et al., 2006), AtNRAMP3 and AtNRAMP4 expression patterns extend to whole cotyledons (Lanquar et al., 2005). The inability to remobilize the low-concentration Fe pool in *nr3nr4vit1-2* (*isv1*), *nr3nr4vit1-3* (*isv2*), and *nr3nr4vit1-1* mutants may account for their more severe phenotypes compared with the *vit1-1* single mutant. Techniques with lower detection limits will be needed to monitor Fe localization and speciation in dry seeds and during germination to solve this issue.

Is Storage in Vacuolar Globoids Bypassed in *nr3nr4vit1-1* Cotyledons?

Here, with TEM-EDX imaging, we conclusively identified the site of Fe storage within cotyledon subepidermal cells and root cortical cells in *vit1-1* as vacuolar globoids. However, there was a discrepancy between the Fe pattern revealed by Perls/DAB staining and the TEM-EDX data for the *nr3nr4vit1-1* triple mutant (Figs. 2, 8, and 9; Supplemental Fig. S1). The pattern revealed by Perls/DAB staining mimicked that of the *vit1-1* mutant. In contrast, TEM-EDX detected similar Fe levels in endodermal and subepidermal cells in the triple mutant (Figs. 8 and 9). This suggests that part of the Fe visualized by Perls/DAB is not associated with vacuolar globoids. This Fe pool may be localized in a different compartment that is too diffuse for detection by TEM-EDX. The more severe phenotype observed in *nr3nr4vit1-1* compared with *vit1-1* during germination might be due to differences in Fe subcellular localization and/or speciation in subepidermal cells in these two mutants (Figs. 8 and 9). In any case, the TEM-EDX data indicate that Fe subcellular localization and/or speciation is distinct in *vit1-1* and *nr3nr4vit1-1*. Determining the identity of the Fe pool in *nr3nr4vit1-1* subepidermal cells will be a challenge for future studies. The difference between *vit1-1* and *nr3nr4vit1-1* observed in dry seeds indicates that AtNRAMP3 and AtNRAMP4 in Fe transport not only during germination but also during embryogenesis. The finding that mutations in transporters involved in vacuolar metal efflux prevent vacuolar Fe storage in subepidermal cells in the *vit1* mutant background is paradoxical. One possibility would be that AtNRAMP3 and AtNRAMP4 are required for Fe transfer between chloroplasts and globoids. During embryo development, Fe is first stored in plastids. Yellow Stripe-Like4 (AtYSL4) and AtYSL6 are involved in Fe efflux from chloroplast. Loss of YSL4

and YSL6 function strongly down-regulates AtNRAMP3 and AtNRAMP4 expression, leading, paradoxically, to Fe sequestration in vacuoles (Divol et al., 2013). A reciprocal regulation may shut down YSL4 and YSL6 expression in *nr3nr4* and lead, paradoxically, to Fe sequestration in plastids. Such a process would occur only in the *vit1-1* background and not in the wild type, because YSL4 and YSL6 are not expressed around vascular tissues (Divol et al., 2013). Testing this hypothesis will require high-resolution temporal and spatial analysis of Fe localization and transport during embryo development.

CONCLUSION

The results reported here demonstrate the functional link between *AtVIT1*, *AtNRAMP3*, and *AtNRAMP4*. These three genes define a functional module active in cells that surround the vasculature in the embryo. The function of this module is essential for optimal seedling establishment under Fe-deficient conditions. Moreover, our data allow a functional dissection of the different Fe pools present in the Arabidopsis embryo and determine their relevance for germination in environments where Fe is poorly available.

MATERIALS AND METHODS

Plant Materials

The generation of Arabidopsis (*Arabidopsis thaliana*) *nr3nr4* and *vit1-1* transfer DNA insertion mutants has been described previously (Kim et al., 2006; Ravet et al., 2009; Molins et al., 2013). To obtain the *nramp3nramp4vit1-1* triple mutant, the *nr3nr4* mutant carrying T-DNA insertions in *AtNRAMP3* (At2G23150) and *AtNRAMP4* (At5G67330) genes was crossed with the *vit1-1* mutant carrying a T-DNA insertion in *AtVIT1* gene (At2G01770), and the F2 progeny was analyzed by PCR genotyping to select homozygous plants at the three loci.

Plant Growth Conditions

Arabidopsis seedlings were grown on ABIS medium [containing 2.5 mM H₃PO₄, 5 mM KNO₃, 2 mM MgSO₄, 1 mM Ca(NO₃)₂, Murashige and Skoog microelements, 1% (w/v) Suc, 1% (w/v) Phytagel (primary root length experiment) or 0.7% (w/v) Phytoagar (all other experiments), and 1 mM MES adjusted with KOH to pH 6.1]. For Fe-sufficient medium, 50 μM FeHBED was added after autoclaving. FeHBED was prepared as a 10 mM stock solution from FeCl₃ (Sigma) and HBED [*N,N'*-di(2-hydroxybenzyl)ethylene diamine-*N,N'*-diacetic acid monochloride hydrate; Strem Chemicals]. HBED was added with a 10% excess to ensure that all Fe was chelated. To deplete the medium of Fe, Fe was omitted (primary root length experiment; -Fe) or Fe was omitted and 50 μM ferrozine [3-(2-pyridyl)-5,6-bis(4-phenyl-sulfonic acid)-1,2,4-triazine] was added to the ABIS medium (all other experiments; -Fe + 50 μM ferrozine). Plates were placed vertically (primary root length experiment) or horizontally (all other experiments) in environmental growth chambers (Sanyo MLR-350) at 21°C with a 16-h photoperiod under 120 μmol photons m⁻² s⁻¹.

EMS-Mutagenized *nr3nr4* Population Production and Screening Conditions

An M0 population of 25,000 seeds of the *nr3nr4* double knockout mutant was treated with 0.15% (v/v) EMS for 16 h and rinsed eight times with about 120 mL and one last time with 500 mL of distilled water to obtain M1 seeds. M1 seeds were sown in pools of 50 per pot and grown in a greenhouse to obtain batches of M2 seeds originating from M1 seed pools. Eight hundred seeds of each M2 batch were sown on two 12- × 12-cm plates (corresponding to a density of five to six seeds

per cm²) containing $-Fe + 50 \mu M$ ferrozine ABIS medium. Seedlings able to grow on this medium were selected after 3, 4, or 7 d of germination and transferred first to Fe-sufficient ABIS medium for recovery and then to pots and grown in the greenhouse to obtain M3 seeds. The inheritance of the suppressor phenotype was then tested by germinating M3 seeds on $-Fe + 50 \mu M$ ferrozine ABIS medium.

Fe Staining in Embryos and Seedlings during Germination

To examine Fe localization in mature embryos and seedlings, Perls/DAB staining was performed according to Roschztardt et al. (2009). Mature embryos were obtained by dissection of seeds that were imbibed in water, in the dark, at 4°C for 1 night. Seedlings used for monitoring Fe mobilization during germination were sown on $-Fe + 50 \mu M$ ferrozine ABIS medium.

Chlorophyll Analysis

After grinding the leaves in liquid nitrogen, pigments were extracted in 1 mL of ethanol at room temperature for 30 min. After centrifugation at 19,000g for 10 min at room temperature, the supernatant was recovered and stored overnight at $-20^{\circ}C$. The supernatant was then centrifuged at 19,000g for 5 min at room temperature, and pigment content was determined spectrophotometrically from the absorbance measured at 534, 643, and 661 nm (Porra et al., 1989).

VIT1 PCR Amplification and Sequencing

Genomic DNA was extracted as described (Edwards et al., 1991). Primers VIT1_for2 (5'-ACCACAAGACATGCAACAAAC-3') and VIT1_rev1 (5'-TTCCCACACACACTTCACAA-3') were used to amplify the coding sequence of the *VIT1* gene. Primers VIT1_for2, VIT1_rev1, VIT1_for3 (5'-GAATCTCTGCCACTTCAG-3'), and VIT1_rev3 (5'-CCTGAAACTGGTAAGACC-3') were used to sequence the PCR amplicon (GATC).

RNA Extraction and RT-PCR Analysis

RNA was extracted from 12 to 15 green siliques using the PowerPlant RNA Isolation Kit (MO BIO Laboratories) following the manufacturer's instructions. DNase treatment was performed by applying 5 μL of RNase-free DNase at 5 units μL^{-1} (MO BIO Laboratories) on the nucleic acid-binding columns. RNA was eluted with 100 μL of RNase-free water. One microgram of RNA was used for RT using the SuperScript III First-Strand Kit (Invitrogen, Thermo Fisher Scientific) with random hexamers. For RT-PCR analysis, VIT1qPCRex1 (5'-CGGAGAAATCGTACGTGACA-3') and VIT1qPCRex4 (5'-GTAACGGTATAAAACCCGCAAAG-3') were used to amplify VIT1 transcripts. Actin2_fwq (5'-GGTAACATTGTGCTCAGTGGTGG-3') and Actin2_revq (5'-AGCATGAAGATTAAGGTCGTT-3') were used to amplify ACTIN2 as a reference. After an initial denaturation step of 5 min at 94°C, PCR amplification proceeded with 35 cycles (*VIT1*) or 25 cycles (*ACTIN2*) of denaturation (30 s at 94°C), hybridization (30 s at 60°C), and extension (30 s at 72°C) and a final extension of 5 min at 72°C.

Functional Expression in Yeast

Saccharomyces cerevisiae strains used in this study were $\Delta ccc1$ (*MATa*; *ura3-53*, *leu2-3,112*, *trp1-1*, *his3-11*, *ade2-1*, *can1-100*, $\Delta ccc1::HIS3$) and the corresponding wild type, DY150 (Li et al., 2001). The mutated VIT1 version (VIT1^{G77D}) was generated using the QuikChange II XL Site-Directed Mutagenesis kit (Stratagene, Agilent Technologies) with mutagenic primers VIT1yeast_3-4-for (5'-CCCATGGAGATAGCATCGGCCCGGACTTCGG-3') and VIT1yeast_3-4_rev (5'-CCGAAGTCGCGGCCGATGCTATCTCCATGGG-3').

$\Delta ccc1$ cells were transformed with either the empty m3838 vector, as a negative control, or plasmids containing VIT1 cDNA from Arabidopsis native or VIT1^{G77D} (fused or not to GFP) under the control of the *Methionine25* promoter by the lithium acetate method (Gietz et al., 1992; Kim et al., 2006). Transformed $\Delta ccc1$ cells were selected on SD-Ura-His medium (Sigma). Complementation of $\Delta ccc1$ was tested by spotting serial dilutions of each yeast strain on SD-Ura medium supplemented or not with 5 or 10 mM FeSO₄. Plates were placed at 30°C for 2 d.

Metal Analyses

For metal analyses in yeast, yeast strains were diluted to an optical density of 0.2 in fresh SD-Ura medium supplemented with 50 μM FeSO₄ and grown for

48 h. After incubation, yeast cultures were placed on ice. Yeast cells were recovered by centrifugation (1,300g, 5 min, and 4°C) and washed first in 50 mL of 10 mM ice-cold EDTA and 50 mM Tris-HCl, pH 6.5, pelleted, and then in ice-cold ultrapure water. For metal analyses in seeds, three or four replicates of about 20 mg of dry seeds were used. All samples were digested in 2 mL of 70% (v/v) nitric acid in a DigiBlock ED36 (LabTech) at 80°C for 1 h, 100°C for 1 h, and 120°C for 2 h. After dilution to 12 mL with ultrapure water, calcium, Fe, magnesium, Mn, and zinc contents of the samples were determined by atomic absorption spectrometry using an AA240FS flame spectrometer (Agilent Technologies).

SXRF Analysis

SXRF computed microtomography data were collected at the GSECARS x-ray microprobe beamline (13-ID-E; Sutton et al., 2002) at the Advanced Photon Source, Argonne National Laboratory. Individual Arabidopsis seeds were glued to 100- μm -diameter quartz capillaries for analysis and mounted vertically and hanging down from the rotational stage above the sample. An incident beam energy of 12 keV from a Si(111) double crystal monochromator (LN₂ cryocooled) was focused to approximately $1 \times 2 \mu m$ (vertical \times horizontal) with reflective rhodium-coated silicon mirrors in a Kirkpatrick-Baez geometry. A four-element silicon-drift diode detector array was used (Hitachi ME-4), coupled to a high-speed digital spectrometer system (XIA XMap), to measure the x-ray μ -fluorescence signal. To collect the x-ray fluorescence sinogram, the seeds were rotated in the focused beam through 363° at an angular speed of 33.333° s⁻¹, saving spectra accumulated through 0.5° every 20 ms. After each full rotation, the seed was stepped horizontally across the beam by 1 μm and then rotated 363° in the opposite direction, generating sinograms consisting of 2,048 energy bins, 727 angles, 501 horizontal steps, and four detector elements (Gürsoy et al., 2015). Tomographic slices of the x-ray fluorescence emission intensities through each seed were computationally reconstructed using filtered back-projection algorithms using procedures written in Interactive Data Language (Exelis VIS).

High-Pressure Freezing, Freeze Substitution, and Embedding

After mechanical removal of the seed integument, the embryos were high-pressure frozen with hexadecane as cryoprotectant in 200- μm -deep carriers with EMPACT2 (Leica Microsystems). Freeze substitution was performed in AFS2 (Leica Microsystems) in 2% (w/v) glutaraldehyde in anhydrous acetone for 4 d, as adapted from Otegui et al. (2002). Samples were infiltrated in Epon at room temperature as follows: 5% (v/v) resin in acetone (4 h), 10% resin (4 h), 25% resin (16 h), and 50%, 75%, and 100% resin (24 h at each concentration). Polymerization was performed at 60°C for 18 h.

Sectioning and EDX Studies

Cotyledons were sectioned along the transverse plane with a 45° HISTO diamond knife (Diatome). Five-hundred-nanometer sections were collected on Formvar carbon-coated 75-mesh copper grids. EDX studies were performed with a JEOL JEM-1400 transmission electron microscope operating at 120 kV and equipped with SAMx silicon drift detector (10 mm²; resolution, 128 eV) with a Peltier cooling system and IDFix software. Spectra were acquired for 120 s at 12,000 magnification at spot size 2 (2- μm beam diameter), with the section tilted 10° toward the detector. Fe data represent the integrated sum of net counts between 6.34 and 6.47 keV (Fe K α 6.4), and Mn data represent those between 5.83 and 5.96 keV (Mn K α 5.9). Net counts were obtained by subtracting the background from the peaks. Two samples per genotype were analyzed. For each section, we analyzed at least five endodermal cells and five subepidermal cells of the abaxial side of cotyledons. For each cell, spectra was obtained on globoids and in the cytosol.

Sequence data from this article can be found in the GenBank/EMBL data libraries under accession numbers NM_127879.3 (AtNRAMP3), NM_126133.3 (AtNRAMP4), and NM_126238.2 (AtVIT1).

Supplemental Data

The following supplemental materials are available.

Supplemental Figure S1. μ PIXE analysis of metal distribution in an *nr3nr4vit1-1* embryo.

Supplemental Figure S2. Alignments of VIT1 RT-PCR amplicon sequences from the wild type and *isv2*.

Supplemental Figure S3. Raw EDX measurements for Fe and Mn in globoids and cytosol.

Supplemental Figure S4. Protein alignment of VIT1 homologs.

Supplemental Table S1. Metal concentrations in seeds measured by atomic absorption spectrometry.

ACKNOWLEDGMENTS

We thank Thiên-Du Chabert for help with the yeast experiments and Antonio Lanzirrotti and Matt Newville for help with data collection and analysis. This work benefited from the facilities and expertise of the Imagif Cell Biology Unit of the Gif campus (<http://www.imagif.cnrs.fr>) which is supported by the Infrastructures en Biologie Sante et Agronomie (IBISA), the French National Research Agency under Investments for the Future programs "France-BioImaging infrastructure" (ANR-10-INSB-04-01), "Saclay Plant Sciences" (ANR-10-LABX-0040-SPS), and the Conseil Général de l'Essonne. This research used resources of the Advanced Photon Source, a U.S. Department of Energy (DOE) Office of Science User Facility operated for the DOE Office of Science by Argonne National Laboratory under Contract No. DE-AC02-06CH11357.

Received March 11, 2015; accepted July 29, 2015; published July 31, 2015.

LITERATURE CITED

- Andrews NC** (2004) Role of Nramp2 (DMT1) in iron homeostasis. *In* M Cellier, P Gros, eds, *The Nramp Family*. Eurekah.com and Kluwer Academic/Plenum, New York, pp 65–68
- Bouis HE** (2003) Micronutrient fortification of plants through plant breeding: can it improve nutrition in man at low cost? *Proc Nutr Soc* **62**: 403–411
- Bruch EM, Thomine S, Tabares LC, Un S** (2015) Variations in Mn(II) speciation among organisms: what makes *D. radiodurans* different. *Metallomics* **7**: 136–144
- Cailliatte R, Schikora A, Briat JF, Mari S, Curie C** (2010) High-affinity manganese uptake by the metal transporter NRAMP1 is essential for *Arabidopsis* growth in low manganese conditions. *Plant Cell* **22**: 904–917
- Clemens S** (2014) Zn and Fe biofortification: the right chemical environment for human bioavailability. *Plant Sci* **225**: 52–57
- Cvitanich C, Przybyłowicz WJ, Urbanski DF, Jurkiewicz AM, Mesjasz-Przybyłowicz J, Blair MW, Astudillo C, Jensen EO, Stougaard J** (2010) Iron and ferritin accumulate in separate cellular locations in *Phaseolus* seeds. *BMC Plant Biol* **10**: 26
- Divol F, Couch D, Conéjéro G, Roschttardt H, Mari S, Curie C** (2013) The *Arabidopsis* YELLOW STRIPE LIKE4 and 6 transporters control iron release from the chloroplast. *Plant Cell* **25**: 1040–1055
- Edwards K, Johnstone C, Thompson C** (1991) A simple and rapid method for the preparation of plant genomic DNA for PCR analysis. *Nucleic Acids Res* **19**: 1349
- Finazzi D, Arosio P** (2014) Biology of ferritin in mammals: an update on iron storage, oxidative damage and neurodegeneration. *Arch Toxicol* **88**: 1787–1802
- Gietz D, St Jean A, Woods RA, Schiestl RH** (1992) Improved method for high efficiency transformation of intact yeast cells. *Nucleic Acids Res* **20**: 1425
- Gollhofer J, Schläwiczke C, Jungnick N, Schmidt W, Buckhout TJ** (2011) Members of a small family of nodulin-like genes are regulated under iron deficiency in roots of *Arabidopsis thaliana*. *Plant Physiol Biochem* **49**: 557–564
- Gollhofer J, Timofeev R, Lan P, Schmidt W, Buckhout TJ** (2014) Vacuolar-Iron-Transporter1-Like proteins mediate iron homeostasis in *Arabidopsis*. *PLoS ONE* **9**: e110468
- Gürsoy D, Biçer T, Lanzirrotti A, Newville MG, De Carlo F** (2015) Hyperspectral image reconstruction for x-ray fluorescence tomography. *Opt Express* **23**: 9014–9023
- Haber F, Weiss J** (1932) On the catalysis of hyperoxide. *Naturwissenschaften* **20**: 948–950
- Hakoyama T, Niimi K, Yamamoto T, Isobe S, Sato S, Nakamura Y, Tabata S, Kumagai H, Umehara Y, Brossuleit K, et al** (2012) The integral membrane protein SEN1 is required for symbiotic nitrogen fixation in *Lotus japonicus* nodules. *Plant Cell Physiol* **53**: 225–236
- Halliwell B** (1978) Superoxide-dependent formation of hydroxyl radicals in the presence of iron chelates: is it a mechanism for hydroxyl radical production in biochemical systems? *FEBS Lett* **92**: 321–326
- Ishikawa S, Ishimaru Y, Igura M, Kuramata M, Abe T, Senoura T, Hase Y, Arao T, Nishizawa NK, Nakanishi H** (2012) Ion-beam irradiation, gene identification, and marker-assisted breeding in the development of low-cadmium rice. *Proc Natl Acad Sci USA* **109**: 19166–19171
- Johnson AA, Kyriacou B, Callahan DL, Carruthers L, Stangoulis J, Lombi E, Tester M** (2011) Constitutive overexpression of the OsNAS gene family reveals single-gene strategies for effective iron- and zinc-biofortification of rice endosperm. *PLoS ONE* **6**: e24476
- Kim SA, Punshon T, Lanzirrotti A, Li L, Alonso JM, Ecker JR, Kaplan J, Guerinet ML** (2006) Localization of iron in *Arabidopsis* seed requires the vacuolar membrane transporter VIT1. *Science* **314**: 1295–1298
- Lanquar V, Lelièvre F, Bolte S, Hamès C, Alcon C, Neumann D, Vansuyt G, Curie C, Schröder A, Krämer U, et al** (2005) Mobilization of vacuolar iron by AtNRAMP3 and AtNRAMP4 is essential for seed germination on low iron. *EMBO J* **24**: 4041–4051
- Lanquar V, Ramos MS, Lelièvre F, Barbier-Brygoo H, Krieger-Liszckay A, Krämer U, Thomine S** (2010) Export of vacuolar manganese by AtNRAMP3 and AtNRAMP4 is required for optimal photosynthesis and growth under manganese deficiency. *Plant Physiol* **152**: 1986–1999
- Li L, Chen OS, McVey Ward D, Kaplan J** (2001) CCC1 is a transporter that mediates vacuolar iron storage in yeast. *J Biol Chem* **276**: 29515–29519
- Lott JN, Spitzer E** (1980) X-ray analysis studies of elements stored in protein body globoid crystals of *Triticum* grains. *Plant Physiol* **66**: 494–499
- McNellis TW, von Arnim AG, Araki T, Komeda Y, Miséra S, Deng XW** (1994) Genetic and molecular analysis of an allelic series of *cop1* mutants suggests functional roles for the multiple protein domains. *Plant Cell* **6**: 487–500
- Molins H, Michelet L, Lanquar V, Agorio A, Giraudat J, Roach T, Krieger-Liszckay A, Thomine S** (2013) Mutants impaired in vacuolar metal mobilization identify chloroplasts as a target for cadmium hypersensitivity in *Arabidopsis thaliana*. *Plant Cell Environ* **36**: 804–817
- Momonoi K, Yoshida K, Mano S, Takahashi H, Nakamori C, Shoji K, Nitta A, Nishimura M** (2009) A vacuolar iron transporter in tulip, TgVIT1, is responsible for blue coloration in petal cells through iron accumulation. *Plant J* **59**: 437–447
- Nevo Y, Nelson N** (2006) The NRAMP family of metal-ion transporters. *Biochim Biophys Acta* **1763**: 609–620
- Otegui MS, Capp R, Staehelin LA** (2002) Developing seeds of *Arabidopsis* store different minerals in two types of vacuoles and in the endoplasmic reticulum. *Plant Cell* **14**: 1311–1327
- Porra R, Thompson W, Kriedemann** (1989) Determination of accurate extinction coefficients and simultaneous equations for assaying chlorophylls a and b extracted with four different solvents: verification of the concentration of chlorophyll II standards by atomic absorption spectroscopy. *Biochim Biophys Acta* **975**: 384–394
- Punshon T, Hirschi K, Yang J, Lanzirrotti A, Lai B, Guerinet ML** (2012) The role of CAX1 and CAX3 in elemental distribution and abundance in *Arabidopsis* seed. *Plant Physiol* **158**: 352–362
- Ravet K, Touraine B, Kim SA, Cellier F, Thomine S, Guerinet ML, Briat JF, Gayard F** (2009) Post-translational regulation of AtFER2 ferritin in response to intracellular iron trafficking during fruit development in *Arabidopsis*. *Mol Plant* **2**: 1095–1106
- Roschttardt H, Conéjéro G, Curie C, Mari S** (2009) Identification of the endosomal vacuole as the iron storage compartment in the *Arabidopsis* embryo. *Plant Physiol* **151**: 1329–1338
- Schnell Ramos M, Khodja H, Mary V, Thomine S** (2013) Using μ PIXE for quantitative mapping of metal concentration in *Arabidopsis thaliana* seeds. *Front Plant Sci* **4**: 168
- Shin JH, Wakeman CA, Goodson JR, Rodionov DA, Freedman BG, Senger RS, Winkler WC** (2014) Transport of magnesium by a bacterial Nramp-related gene. *PLoS Genet* **10**: e1004429
- Sutton SR, Bertsch PM, Newville M, Rivers ML, Lanzirrotti A, Eng PJ** (2002) Microfluorescence and microtomography analyses of heterogeneous earth and environmental materials. *In* PA Fenter, ML Rivers, NC Sturchio, SR Sutton, eds, *Applications of Synchrotron Radiation in Low-Temperature Geochemistry and Environmental Science*, Vol 49. Mineralogical Society of America, Chantilly, VA, pp 429–483
- World Health Organization** (2015) *The Global Prevalence of Anemia in 2011*. World Health Organization, Geneva
- Xia J, Yamaji N, Kasai T, Ma JF** (2010) Plasma membrane-localized transporter for aluminum in rice. *Proc Natl Acad Sci USA* **107**: 18381–18385
- Zhang Y, Xu YH, Yi HY, Gong JM** (2012) Vacuolar membrane transporters OsVIT1 and OsVIT2 modulate iron translocation between flag leaves and seeds in rice. *Plant J* **72**: 400–410